Title

Receptor Induced Doping of Conjugated Polymer Transistors: A Strategy for Selective and Ultrasensitive Phosphate Detection in Complex Aqueous Environments

Journal

Advanced Electronic Materials, 8(7)

ISSN

2199-160X

Authors

Benasco, Anthony R
Tropp, Joshua
Kaphle, Vikash
et al.

Publication Date

2022-07-01

DOI

10.1002/aelm.202101353

Peer reviewed

ADVANCED ELECTRONIC MATERIALS
www.advelectronicmat.de

Receptor Induced Doping of Conjugated Polymer Transistors: A Strategy for Selective and Ultrasensitive Phosphate Detection in Complex Aqueous Environments

*Anthony R. Benasco, Joshua Tropp, Vikash Kaphle, Yusheng Chen, Wei Zhao, Naresh Eedugurala, Tse Nga Ng, Amar H. Flood, and Jason D. Azoulay**

Phosphate oxyanions play central roles in biological, agricultural, industrial, and ecological processes. Their high hydration energies and dynamic properties present a number of critical challenges limiting the development of sensing technologies that are cost-effective, selective, sensitive, field-deployable, and which operate in real-time within complex aqueous environments. Here, a strategy that enables the fabrication of an electrolyte-gated organic field-effect transistor (EGOFET) is demonstrated, which overcomes these challenges and enables sensitive phosphate quantification in challenging aqueous environments such as seawater. The device channel comprises a composite layer incorporating a diketopyrrolopyrrole-based semiconducting polymer and a π-conjugated penta-*t*-butylpentacyanopentabenzo[25]annulene "cyanostar" receptor capable of oxyanion recognition and embodies a new concept, where the receptor synergistically enhances the stability and transport characteristics via doping. Upon exposure of the device to phosphate, a current reduction is observed, consistent with dedoping upon analyte binding. Sensing studies demonstrate ultrasensitive and selective phosphate detection within remarkably low limits of detection of 178×10^{-12} M (17.3 parts per trillion) in buffered samples and stable operation in seawater. This receptor-based doping strategy, in conjunction with the versatility of EGOFETs for miniaturization and monolithic integration, enables manifold opportunities in diagnostics, healthcare, and environmental monitoring.

1. Introduction

Phosphate oxyanions play central roles in biological, agricultural, industrial, and ecological processes.[1,2] As a principal constituent of biological systems, phosphate is industrially relevant in the production of medicinal drugs, pharmaceuticals, therapies, and is crucial to the growth of plants and animals.[3] Phosphate oxyanions also serve as potent environmental pollutants responsible for the eutrophication of natural water sources leading to hypoxia, fish kills, and "dead zones."[1,4] The development of low-cost, selective, and real-time sensors that operate in complex aqueous environments remains a significant challenge, precluding the development of critical sensing technologies such as those related to biomedicine, environmental monitoring, and point-of-need testing.[5] Current methods of nutrient quantification necessitate sample collection, extraction, and enrichment followed by colorimetric analyses or laboratory-based spectrophotometric, fluorescent, and chromatographic methods.[6,7] Portable ion-selective electrodes (ISEs) offer the opportunity for real-time monitoring; however, the hydrated nature and dynamic properties of these anions result in cross-interference,[8] limiting their accurate quantification at relevant concentrations (0.02×10^{-6}–2×10^{-6} M) in freshwater and seawater.[6] The need for improved analytical performance, miniaturization, in situ operation, and access to spatially and temporally representative data has driven the development of solid-state potentiometric, chemiresistive, amperometric, capacitive, and field-effect transistor sensor platforms.[9] In these devices, specificity is derived from molecular recognition elements such as ion-selective membranes, molecularly imprinted polymers, biomacromolecules, and small-molecule receptors.[10–12] Despite the exploration of a vast chemical space and advancements in device design, the specificity and sensitivity required for trace detection of these anions have yet to be achieved.

Label-free organic electronic sensors based on organic field-effect transistor (OFET) architectures offer novel attributes that match the needs of emerging sensor platforms.[12–14] These

A. R. Benasco, J. Tropp, V. Kaphle, N. Eedugurala, J. D. Azoulay
Center for Optoelectronic Materials and Devices
School of Polymer Science and Engineering
University of Southern Mississippi
Hattiesburg, MS 39406, USA
E-mail: jason.azoulay@usm.edu
Y. Chen, W. Zhao, A. H. Flood
Department of Chemistry
Indiana University
800 East Kirkwood Avenue, Bloomington, IN 47405, USA
T. N. Ng
Department of Electrical and Computer Engineering
University of California San Diego
9500 Gilman Drive, La Jolla, CA 92093-0407, USA

The ORCID identification number(s) for the author(s) of this article can be found under https://doi.org/10.1002/aelm.202101353.

DOI: 10.1002/aelm.202101353

include low-cost fabrication on diverse substrates, synthetic tunability, mechanical compliance, and direct integration with existing signal processing electronics, enabling monolithic sensing systems.[15] Furthermore, OFET-based sensors offer improved sensitivity resulting from amplification endowed by the field-effect, the integration of chemical probes at the surface, channel, or electrodes of the device, and high diversity in device architecture. These attributes have advanced OFET-based sensors to the forefront of environmental, biomedical, and wearable diagnostics platforms. Among these, electrolyte-gated OFETs (EGOFETs) are promising for in situ monitoring since they directly transduce interfacial phenomena such as molecular recognition events into electrical signals with ultra-high sensitivity.[14] While these transistors can be endowed with selectivity through various functionalization strategies, it remains a challenge to electronically couple such receptor chemistries to the active materials of these devices.[15] Furthermore, the integration of many host–guest chemistries into transistors comes at the cost of reduced device performance and a loss of both stability and selectivity in complex aqueous environments.

Over the past two decades, there have been remarkable breakthroughs in the design and synthesis of supramolecular receptors capable of host–guest oxyanion complexation.[16] In particular, penta-*t*-butylpentacyanopentabenzo[25]annulene "cyanostar" (CS) demonstrates high-fidelity binding of larger anions such as $H_2PO_4^-$ within its electropositive, size-selective cavity by virtue of aromatic C-H hydrogen bonding interactions (**Figure 1**).[17,18] CS has been utilized as an ionophore[19] but has not been leveraged in an OFET architecture to endow selectivity. Here, we describe the development of an EGOFET comprised of a composite layer of a semiconducting polymer poly[2,5-bis(2-decyltetradecyl)pyrrolo[3,4-*c*]pyrrole-1,4-(2*H*,5*H*)-dione-*alt*-(*E*)-1,2-di(2,2'-bithiophen-5-yl)ethene] (PDVT) and CS

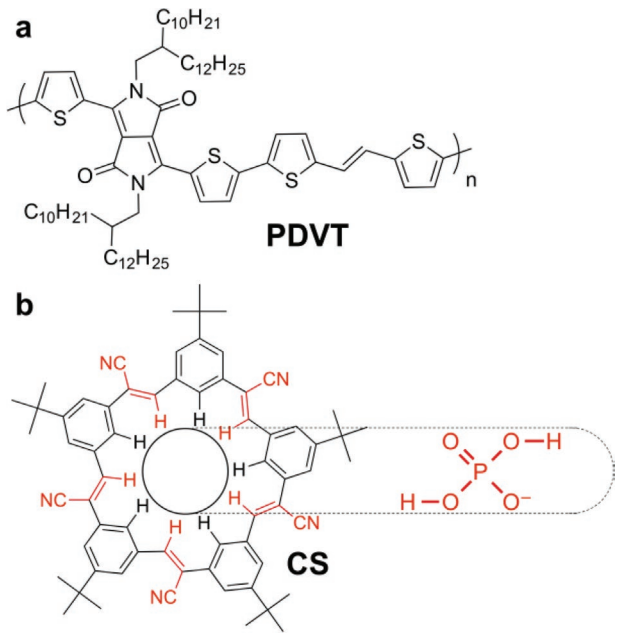

Figure 1. a) Molecular structures of the semiconducting polymer (PDVT) and b) cyanostar receptor (CS) which can bind phosphate.

(Figure 1) that enables the detection of oxyanions within complex aqueous environments. Crucial aspects of the sensor, such as high environmental stability and oxyanion recognition, are achieved using a new strategy in which CS dopes the semiconducting polymer. In the presence of analytes, CS preferentially binds phosphate, resulting in dedoping and large changes to the electrical properties that are compatible with digital readout methods. The robust nature of the electronic doping-dedoping phenomena is demonstrated in complex aqueous environments such as seawater and is therefore amenable for the real-time selective detection of phosphate oxyanions.

2. Results and Discussion

The conjugated polymer PDVT was chosen on the basis of its high field-effect mobility (μ), excellent film-forming properties, and environmental stability.[20] Both PDVT and CS feature rigid extended π-systems that promote strong intermolecular and solid-state interactions, indicative of their potential for electronic coupling. The polymer was synthesized using a microwave-assisted Stille cross-coupling copolymerization resulting in a number average molecular weight (M_n) of 43.7 kg mol^{-1} and dispersity ($Đ$) of 2.14 (Figure S1, Supporting Information). Mixtures of the polymer and receptor were initially examined using UV–vis–NIR and electron paramagnetic resonance (EPR) spectroscopies. Thin films for UV–vis–NIR studies were prepared by spin-coating chlorobenzene mixtures of the polymer (10 mg mL^{-1}) and CS (1:1 w/w% relative to polymer) onto quartz substrates. An absorption maximum (λ_{max}) at 804 nm in the pristine PDVT is consistent with aggregation from π–π stacking. The solid-state absorption of PDVT-CS displayed a modest blueshift of 11 and 6 nm at the 0–0 and 0–1 vibronic peaks, a concomitant lowering of the relative intensity of these transitions (PDVT-CS: I_{0-0}/I_{0-1} = 1.07, PDVT: I_{0-0}/I_{0-1} = 1.24), and the presence of a low energy absorption tail (**Figure 2**a). The decrease of intensity of the π–π stacking peak can be associated with a partial disruption of polymer chain interactions and solid-state ordering.[21] These data further suggest the formation of a ground-state charge-transfer complex from the electronic coupling between the PDVT and CS.[22] Further details regarding optical and electrochemical characterization can be found in Figure S2 and Table S1 in the Supporting Information.

EPR spectroscopy was used to investigate the doping phenomena. Films were prepared by evaporating chloroform solutions of PDVT and PDVT-CS in 4 mm quartz EPR tubes using the same CS loading as the UV–vis–NIR films. While PDVT films and CS showed no signal (Figure S4a,b, Supporting Information), PDVT-CS films displayed a broad, single line at a *g*-factor (*g*) of 2.0034, indicating the formation of paramagnetic species (Figure 2b,c and Table S2, Supporting Information) by doping. Doping was also supported by Kelvin probe force microscopy (KPFM) measurements, which demonstrate a considerable shift in the PDVT Fermi level upon the addition of CS (Figure S5, Supporting Information).[23] CS macrocycles offer novel anion recognition capabilities on account of their propensity to bind and stabilize anions (Figure S35, Supporting Information).[24] As such, organic-soluble tetrabutylammonium dihydrogen phosphate (TBAP, 1 equiv. relative

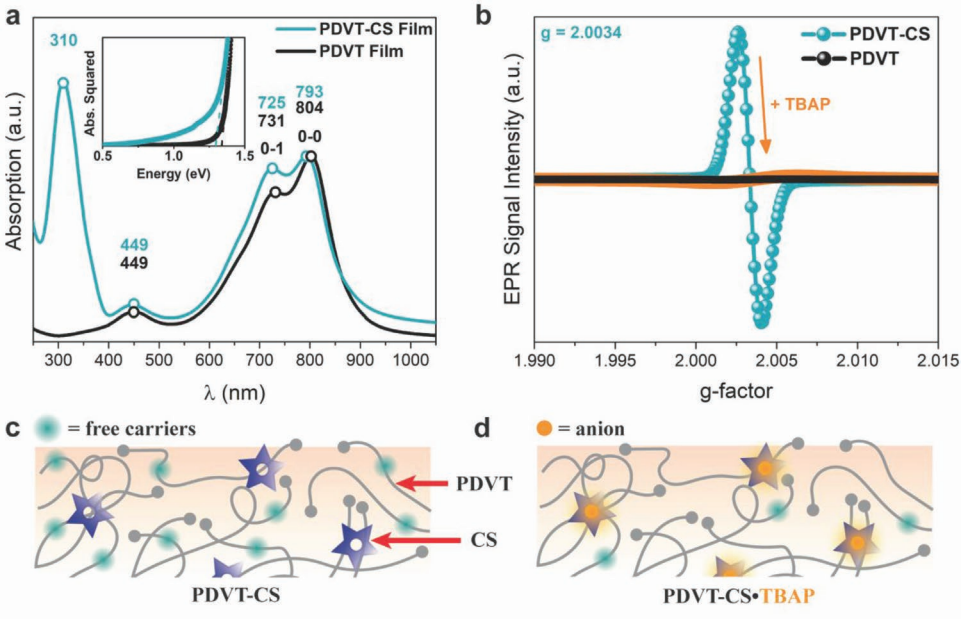

Figure 2. a) UV–vis–NIR absorption profile of pristine PDVT and PDVT-CS films spin-coated from chlorobenzene onto quartz substrates. The inset illustrates a pronounced low-energy absorption tail upon CS addition. b) EPR (X-band) spectra at room temperature of PDVT-CS demonstrating the formation of paramagnetic species, consistent with c) doping. Upon addition of tetrabutylammonium dihydrogen phosphate (TBAP, 1 equiv. relative to CS) to PDVT-CS the films show predominantly diamagnetic behavior, consistent with d) dedoping.

to CS) was mixed with PDVT-CS, which resulted in a dramatic reduction in the EPR signal and predominantly diamagnetic behavior (Figure 2b,d). Taken together, the PDVT-CS combination demonstrates an anion-induced electronic transition which presents itself as a design paradigm for the chemical sensing of phosphate.

OFETs have demonstrated utility in a large number of consumer technologies and show unparalleled modularity in sensing a wide variety of biological, chemical, and physical analytes.[25] Thus, PDVT and CS were combined and utilized as the active layer within the channel of an OFET in order to investigate whether the previously observed doping phenomena could be translated into a signal transduction mechanism and applied for anion sensing. PDVT-CS films (CS loading = 0, 4, 10, 20 wt%) were spin-coated onto *n*-octadecyltrichlorosilane-treated SiO_2/Si substrates (electrodes: Cr ≈ 5 nm, Au ≈ 60 nm, length (L) = 80 µm and channel width (W) = 1 mm) to construct bottom-gate, bottom-contact (BGBC) devices (**Figure 3**a). Figure 3b–d shows the room-temperature conductivities (σ_{RT}) obtained using two-point probe measurements and OFET transfer and output characteristics for neat PDVT and PDVT-CS (20 wt%) composite films. Further details on the fabrication, solution processing, and testing parameters are discussed in the Supporting Information.

All devices demonstrated p-type FET behavior. The neat PDVT films displayed an average hole mobility of 2.95×10^{-2} cm^2 V^{-1} s^{-1} and on/off current ratio (I_{on}/I_{off}) of ≈10^6. Low loadings of 1–2 wt% CS are pinned to a trap-limited doping regime,[12,26] while a critical threshold of 4 wt% CS was found to produce linear I–V characteristics consistent with Ohmic transport. A concomitant increase in σ_{RT} was evident upon increasing the CS concentration. Loadings of 4, 10, and 20 wt% CS result in σ_{RT} of 1.17×10^{-5}, 1.75×10^{-4}, and 8.20×10^{-3} S cm^{-1}, respectively. The PDVT-CS transfer curves do not demonstrate an off-state (Figure 3c), indicating the presence of free carriers, consistent with EPR studies, and a lowering of the gate-dependent channel conduction. There was a concomitant increase in μ up to 3.43×10^{-2} cm^2 V^{-1}s^{-1} for the 20 wt% CS devices. The enhancement of carrier mobility, with increasing CS loading, is unique and emanates from doping since all prior reports generally demonstrate deleterious effects on mobility upon the incorporation of receptor chemistries into organic semiconductors.[27] The carrier concentration (n) was calculated from the mobility using the equation $\sigma = nq\mu$, where q is the elementary charge (Table S4, Supporting Information). The addition of CS correlates with a proportional increase in σ_{RT} with n increasing from 10^{15} cm^{-3} (neat PDVT) to greater than 10^{18} cm^{-3} at 20 wt% CS.

The Ohmic transport of the composite systems can be associated with the presence of free carriers introduced by doping and the modified injection barrier at the electrode-semiconductor junction.[28] As such, variable temperature (180–340 K) mobility and transmission line method (TLM) measurements were performed to extract the activation energy (E_a) and the contact resistance (R_C), respectively. The temperature dependence of μ originates from a thermally activated process described by the relation $\mu(T) = \mu_0 \exp(-E_a/k_B T)$, where μ_0 is a pre-exponential factor, k_B is the Boltzmann constant, and T denotes the temperature. The values for E_a of 78 meV (PDVT-CS) < E_a = 113 meV (PDVT) ($\Delta E_a \approx 35$ meV) are consistent with a reduced energetic barrier for charge transport. The TLM results suggest a reduction of the contact resistance (R_C = 4.5 MΩ) consistent with doping and change in surface potential observed by KPFM (Figure S5, Supporting Information).[29] Therefore, despite

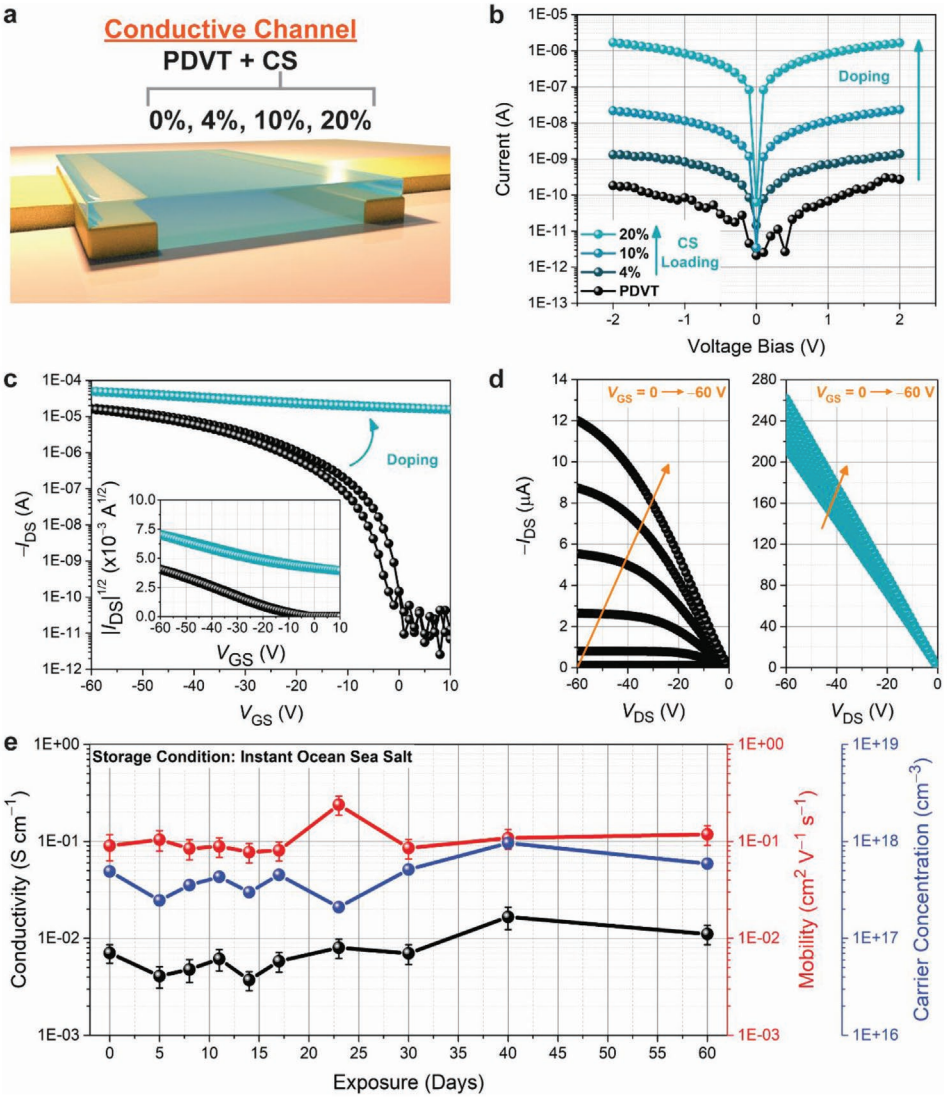

Figure 3. a) Schematic illustration of a bottom-gate bottom-contact (BGBC) device structure. PDVT-CS devices (CS loading = 0, 4, 10, and 20 wt%) were fabricated and tested to evaluate electronic transformations, material compatibility, and storage stability. b) Electrical conductivities obtained from two-point probe measurements (−2 to 2 V) of PDVT-CS films. c) FET transfer characteristics and d) output curves (left) without and (right) with CS (20 wt%) showing enhancement in *p*-channel operation using source and drain electrodes (L = 80 μm, W = 1 mm). e) Monitoring of device stability for high performing PDVT-CS films over 60 d. Films were completely submerged in Instant Ocean Sea Salt electrolyte (in the absence of light) and showed minimal changes in the conductivity (black), field-effect mobility (red), and carrier concentration (blue).

producing kinetically quenched morphologies from spin-coating, the composite systems do not appear to be hampered by non-interactive interfaces formed at the electrode-semiconductor junction.[30] To investigate the electrical stability of the PDVT-CS transistors, devices were monitored under an atmosphere of nitrogen in the dark, in ambient conditions, in ultrapure deionized (DI) water, and in Instant Ocean Sea Salt electrolyte. In all cases, the devices exhibit excellent storage stability over a 60 d testing period, even when completely submerged into Instant Ocean Sea Salt electrolyte (Figure 3e), a rare demonstration that is essential for practical translation to field use.[10,31]

We sought to translate the electronic behavior observed for PDVT-CS mixtures exposed to TBAP (Figure 2b) by incorporating the composite into an OFET architecture. Anions were directly embedded into the PDVT-CS composite matrix to investigate anion-induced electronic perturbations. Adopting the original protocols for device fabrication and testing (Figure 3a–d), organic-soluble tetrabutylammonium salts (TBAX, where X = dihydrogen phosphate (P), nitrate (N), chloride (Cl), perchlorate (PC), and hydrogen sulfate (HS)) were added to PDVT-CS chlorobenzene solutions (1 equiv. relative to CS) for competitive binding measurements. The anions listed were selected based on their vital role and prevalence in ecosystems and agriculture.[32] The binding of anions by CS in low dielectric solvents is an electrostatically driven process, which takes place inside the central cavity ($d_{cavity} \approx 4.5$ Å) and arises from activated C–H hydrogen-bonding units.[17] The solvent choice (chlorobenzene, $\varepsilon = 5.62$) and the sequential film casting into

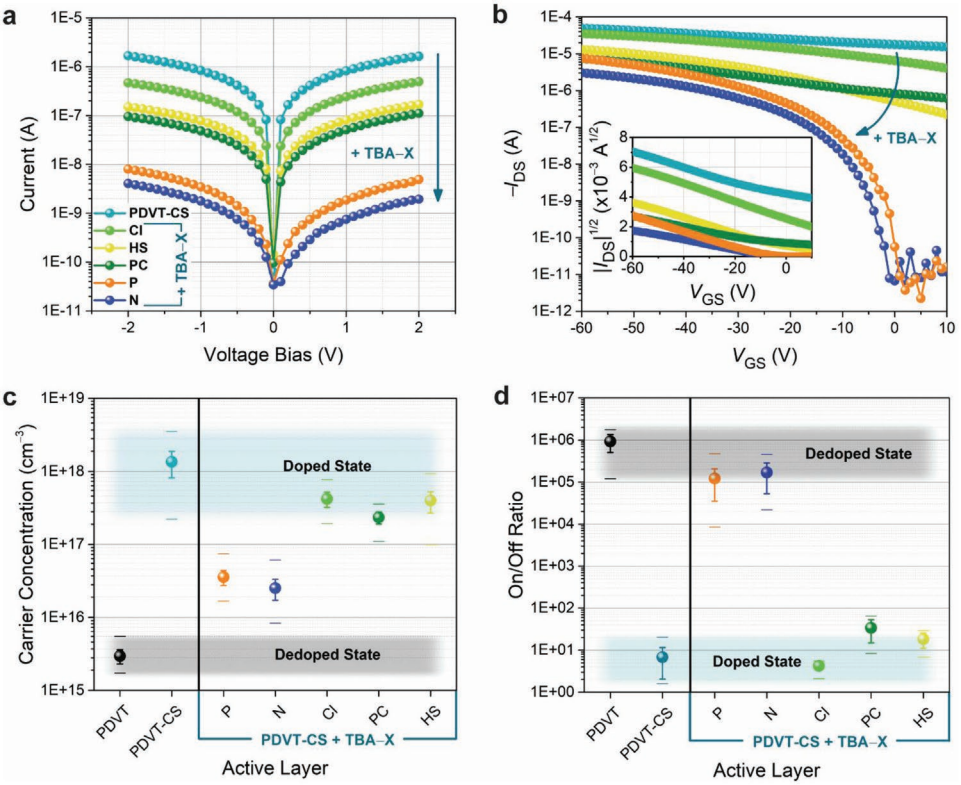

Figure 4. OFET devices (BGBC configuration) based on a three-component mixture of PDVT-CS•TBAX salts (X = P, N, Cl, PC, and HS) and their associated a) two-point probe *I–V* characteristics and b) OFET transfer curves. The variation in the dedoping response and the preservation of charge transport characteristics without degradation demonstrates that receptor-anion interactions dictate the magnitude of charge carrier reduction. c) Summary of carrier concentration (cm^{-3}) within the conductive channel and d) OFET on/off current ratio comparing ten independent devices with source and drain electrode geometries of $L = 80$ µm and $W = 1$ mm.

an OFET architecture introduces the appropriate conditions to monitor the analyte's preferential interactions, whether toward the receptor or polymer chain.

Both σ_{RT} and μ measurements reveal anion composition-dependent channel conduction and offsets from the original PDVT-CS film properties (dedoping) (**Figure 4**). The TBAP and tetrabutylammonium nitrate (TBAN) films, in particular, displayed the highest reduction (> 2 orders of magnitude) in bulk channel conduction with $\sigma_{RT} = 3.55 \times 10^{-5}$ and 5.28×10^{-5} S cm^{-1} and in carrier density with $n = 5.24 \times 10^{16}$ and 2.49×10^{16} cm^{-3}, respectively (Figure 4a,c). These characteristics coincide with the high on–off current ratios ($I_{on}/I_{off} > 10^5$) (Figure 4b,d) and closely mirror the native PDVT profile (Figure 3c). On the other hand, σ_{RT} values only moderately decreased to 3.09×10^{-3} S cm^{-1} (TBACl), 4.86×10^{-4} S cm^{-1} (tetrabutylammonium perchlorate), and 6.40×10^{-4} S cm^{-1} (tetrabutylammonium hydrogen sulfate) and similar carrier concentrations were obtained with $n = 4.59 \times 10^{17}$, 2.40×10^{17}, and 1.54×10^{17} cm^{-3}, respectively. To ensure these anion interactions are preferential to the receptor, TBAP and TBAN were separately added to PDVT (without CS) to assess how it alters the transfer profile. Both conditions degraded the PDVT *p*-channel operation once introduced (Figure S19, Supporting Information) and support the notion of receptor-anion host–guest complexation as the dominant factor in the dedoping responses. Collectively, the electrical characterization techniques correlate to the diamagnetic behavior found in EPR studies (Figure 2b). Due to the weak nature of intermolecular interactions, the host–guest complexation of CS resulted in a perturbation of the electronic structure or diminished steric interactions with the π-system. This robust phenomenon manifests as a dramatic change in electrical properties only in the presence of specific anions.

To investigate whether the observed anion selectivity in the OFET configuration could be translated to a real-time aqueous sensor, water-soluble sodium salts of the previously tested anions were introduced to the PDVT-CS film within an aqueous electrolyte (HEPES, pH = 7.4), (**Figure 5**a). In this EGOFET configuration, the Ag/AgCl gate was electrically coupled to the composite film via the electrolyte solution, which was then spiked with the anion salt of interest. The gate electrode bias facilitates ion migration toward the channel interface with no bulk volumetric response due to the hydrophobic nature of the film (Figure S20, Supporting Information). Further details regarding EGOFET fabrication can be found in the Supporting Information. While PDVT-CS films remained stable when tested under various pH conditions (4–10, Figure S21, Supporting Information), HEPES buffer (baseline) solution showed consistent output responses (Figure S22, Supporting Information) and was used to maintain consistent sensing environments between each analyte (Figure S23, Supporting Information). Baseline measurements were first conducted by monitoring the drain current (I_{DS}) drift upon continuous exposure to an aqueous solution with no target

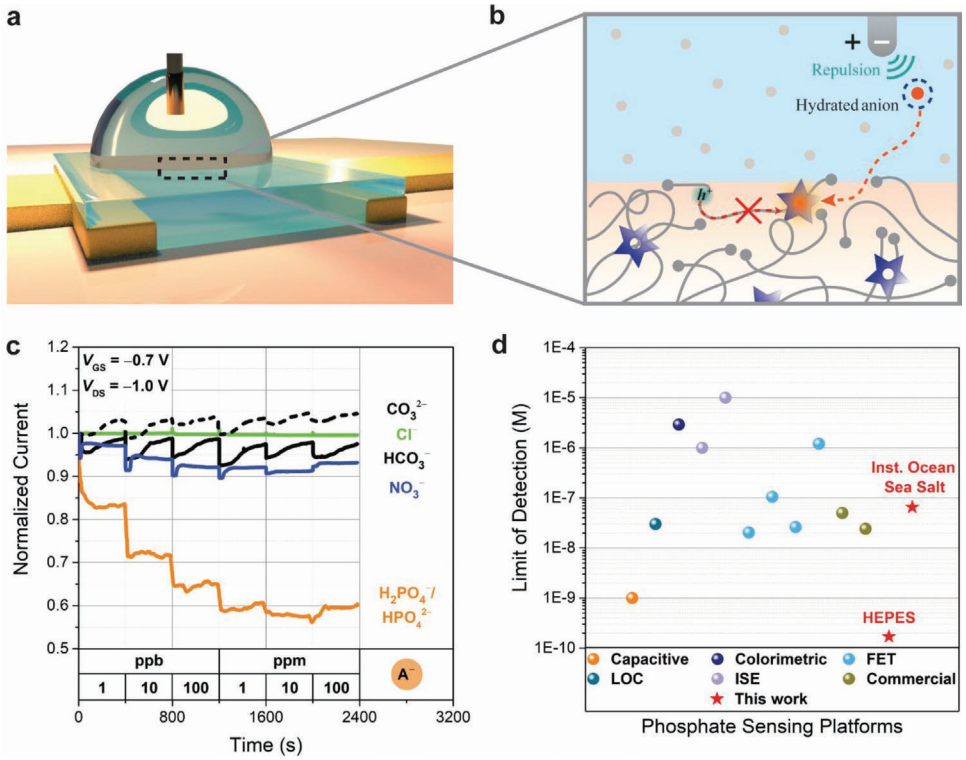

Figure 5. a) Schematic illustration of the EGOFET device and b) the proposed sensing mechanism. c) Transient responses of the device toward phosphate ($H_2PO_4^-/HPO_4^{2-}$), nitrate (NO_3^-), bicarbonate (HCO_3^-), carbonate (CO_3^{2-}), and chloride (Cl^-) in HEPES buffer (pH = 7.4). d) Comparison of state-of-the-art phosphate sensors with PDVT-CS, which demonstrated a limit of detection (LOD) and quantification (LOQ) of 178×10^{-12} M (17.3 parts per trillion (ppt)) and 430×10^{-12} M (41.7 ppt), respectively.

analyte present. Next, the transient responses toward dissolved sodium salts of phosphate ($H_2PO_4^-$), nitrate (NO_3^-), bicarbonate (HCO_3^-), carbonate (CO_3^{2-}), and chloride Cl^- at various concentrations (nM–mM) were measured and compared to the baseline trend so as to determine the channel current offset and the resultant chemical sensing performance (Figure S24, Supporting Information). The sensitivity (S) is defined by the relative change of the drain current under the same voltage conditions (V_{GS} = −0.7 V and V_{DS} = −1.0 V) following the equation[33]

$$S = \frac{|I_{DS}(analyte) - I_{DS}(baseline)|}{I_{DS}(baseline)} \times 100 \quad (1)$$

Upon analyte introduction, the electrical response to phosphate anions emanates from migration to the film interface (<1 nm film swelling exposed to DI water, Figure S20, Supporting Information), leading to physical adsorption and channel conduction changes. In this case, receptor-analyte complexation generated a dedoping response as a function of anion concentration, which matches the results from the three-component films (Figure 4). The limit of detection (LOD) and quantification (LOQ) were calculated from the noise of each sensor as previously reported (Figure S25, Supporting Information).[34,35] From the calibration plot for phosphate, the LOD and LOQ were calculated to be 178×10^{-12} M (17.3 ppt) and 430×10^{-12} M (41.7 ppt), respectively. The observed sensitivity is competitive with diverse classes of state-of-the-art phosphate sensors including capacitive,[36] colorimetric,[37] lab-on-chip,[38] ISEs,[39] FETs,[34,40] and commercialized products (Figure 5d and Table S8, Supporting Information).

The selectivity was investigated by individually challenging the device with other mono- and divalent anions comprising NO_3^-, SiO_3^{2-}, Br^-, HCO_3^-, CO_3^{2-}, SO_4^{2-}, and Cl^- (Figure 5c and Figures S24–S26, Supporting Information). Overall, the transient responses revealed a more pronounced reduction in the bulk channel conduction upon exposure to phosphate when compared to the other anions tested. Calibration and sensitivity metrics for each anion can be found in Figures S24–S26 in the Supporting Information. To further support the CS-dependent selective dedoping of the real-time sensor, EGOFETs were fabricated and tested with photoisomerized IsoCS (Figures S3 and S9 and Table S5, Supporting Information), rather than CS. The solution NMR of IsoCS (Figures S27–S29, Supporting Information) and sequential PF_6^- anion titration experiments (Figures S30–S32, Supporting Information) suggested a lack of anion affinity. Moreover, aqueous sensors using PDVT-IsoCS active layers were electrochemically unstable and no statistically significant electrical responses were observed upon anion addition (Figure S33, Supporting Information). Taken together, the anion-selective dedoping response of the device was dependent on the shape-persistent electropositive cavity of the CS, rather than other possible interactions with PDVT.

To demonstrate the potential for real-time phosphate oxyanion detection in the marine environment, we tested the PDVT-CS EGOFETs in high ionic strength, artificial seawater solution (Instant Ocean Sea Salt electrolyte). This mixture gives

a typical salinity of 35 parts per thousand and contains appreciable concentrations of ions prevalent in seawater (>1 ppm): Na^+, K^+, Mg^{2+}, Ca^{2+}, Sr^{2+}, Br^-, Cl^-, CO_3^{2-}, HCO_3^-, and SO_4^{2-}. The transient responses toward the dissolved sodium salt of phosphate at various concentrations (nM–mM) were measured using the same conditions employed for measurements in HEPES buffer. The LOD and LOQ in artificial seawater were 65.4×10^{-9} M (6.54 parts per billion (ppb) and 940×10^{-9} M (91.2 ppb), respectively (Figure S34, Supporting Information). The measured sensitivity (Figure 5d and Figures S25 and S34, Supporting Information) and seawater stability (Figure 3e) are competitive with current technologies (Figure S38 and Table S8, Supporting Information), demonstrating the utility of our approach for the real-time selective detection of phosphate oxyanions.

3. Conclusion

In summary, we have demonstrated a new strategy for the selective detection of phosphate, an anion with central roles in biological, agricultural, industrial, and ecological processes. This was enabled by the combination of the semiconducting polymer PDVT with CS. This synergistic combination offered engineered electronic interactions that result in doping and unparalleled stability in water, selective phosphate complexation by the receptor in the presence of competing anions, and a significant dedoping of the polymer in the presence of phosphate. Spectroscopic analysis suggests the doping was promoted by weak orbital mixing of PDVT and CS, forming a ground-state charge-transfer complex sensitive to electronic and structural perturbations induced by analyte binding. When the active layer was mixed with TBA salts of various anions, the device transfer and *I–V* characteristics demonstrate a selective and strong dedoping response toward phosphate. This selectivity was then translated to an EGOFET for real-time experiments, which demonstrated ultrasensitive phosphate detection with a LOD of 178×10^{-12} M (17.3 ppt) in buffered samples, well within the U.S. Environmental Protection Agency specifications. The device also demonstrated the stable, selective, and sensitive detection of phosphate in artificial seawater, a rare demonstration and critical step toward practical field deployment. The unmatched performance of this sensor and new strategy for analyte detection overcome significant challenges and offer a novel approach for phosphate detection within complex aqueous environments. In a broader context, the combination of semiconducting polymers with next-generation receptors offers manifold opportunities for designing novel composite films that can be applied within emerging OFET-based diagnostic, healthcare, environmental monitoring, and bioelectronics platforms.

Supporting Information

Supporting Information is available from the Wiley Online Library or from the author.

Acknowledgements

The work performed at the University of Southern Mississippi was supported by the National Science Foundation (OIA-1632825) and the Office of Naval Research (N00014-19-1-2687). A.H.F. acknowledges support from the National Science Foundation (CHE 2105848). The 500 MHz NMR spectrometer of the Indiana University NMR facility was supported by National Science Foundation grant CHE-1920026 and the Prodigy probe was purchased in part with support from the Indiana Clinical and Translational Sciences Institute funded, in part by National Institutes of Health Award TL1TR002531.

Conflict of Interest

The authors declare no conflict of interest.

Data Availability Statement

The data that support the findings of this study are available in the Supporting Information of this article.

Keywords

chemical sensing, conjugated polymer, cyanostar macrocycle, organic field-effect transistor, water quality monitoring

Received: December 12, 2021
Revised: February 10, 2022
Published online:

[1] D. L. Correll, *J. Environ. Qual.* **1998**, *27*, 261.
[2] a) T. Tyrrell, *Nature* **1999**, *400*, 525; b) K. G. Raghothama, *Annu. Rev. Plant Biol.* **1999**, *50*, 665.
[3] a) D. Cordell, J.-O. Drangert, S. White, *Global Environ. Change* **2009**, *19*, 292; b) S. M. Moe, *Primary Care* **2008**, *35*, 215.
[4] a) S. R. Carpenter, N. F. Caraco, D. L. Correll, R. W. Howarth, A. N. Sharpley, V. H. Smith, *Ecol. Appl.* **1998**, *8*, 559; b) V. H. Smith, *Environ. Sci. Pollut. Res.* **2003**, *10*, 126.
[5] a) G. Duffy, F. Regan, *Analyst* **2017**, *142*, 4355; b) M. Cuartero, *Sens. Actuators, B Chem.* **2021**, *334*, 129635; c) X. Zhu, J. Ma, *Trends Anal. Chem.* **2020**, *127*, 115908; d) C. Warwick, A. Guerreiro, A. Soares, *Biosens. Bioelectron.* **2013**, *41*, 1; e) A. T. Law al, S. B. Adeloju, *Talanta* **2013**, *114*, 191.
[6] M. A. P. Mahmud, F. Ejeian, S. Azadi, M. Myers, B. Pejcic, R. Abbassi, A. Razmjou, M. Asadnia, *Chemosphere* **2020**, *259*, 127492.
[7] a) M. D. Patey, M. J. A. Rijkenberg, P. J. Statham, M. C. Stinchcombe, E. P. Achterberg, M. Mowlem, *Trends Anal. Chem.* **2008**, *27*, 169; b) A. K. Williams, J. Tropp, E. R. Crater, N. Eedugurala, J. D. Azoulay, *ACS Appl. Polym. Mater.* **2019**, *1*, 309.
[8] a) M. Cuartero, G. A. Crespo, *Curr. Opin. Electrochem.* **2018**, *10*, 98; b) M. J. Langton, C. J. Serpell, P. D. Beer, *Angew. Chem.* **2016**, *55*, 1974.
[9] a) M. Y. Mulla, E. Tuccori, M. Magliulo, G. Lattanzi, G. Palazzo, K. Persaud, L. Torsi, *Nat. Commun.* **2015**, *6*, 6010; b) L. Torsi, M. Magliulo, K. Manoli, G. Palazzo, *Chem. Soc. Rev.* **2013**, *42*, 8612; c) U. Lange, V. M. Mirsky, *Anal. Chim. Acta* **2011**, *687*, 105.
[10] O. Knopfmacher, M. L. Hammock, A. L. Appleton, G. Schwartz, J. Mei, T. Lei, J. Pei, Z. Bao, *Nat. Commun.* **2014**, *5*, 2954.
[11] a) M. Cuartero, E. Bakker, *Curr. Opin. Electrochem.* **2017**, *3*, 97; b) J. Wang, R. Liang, W. Qin, *Trends Anal. Chem.* **2020**, *130*, 115980.
[12] H. Li, W. Shi, J. Song, H.-J. Jang, J. Dailey, J. Yu, H. E. Katz, *Chem. Rev.* **2019**, *119*, 3.
[13] J. Rivnay, S. Inal, A. Salleo, R. M. Owens, M. Berggren, G. G. Malliaras, *Nat. Rev. Mater.* **2018**, *3*, 17086.

[14] F. Torricelli, D. Z. Adrahtas, Z. Bao, M. Berggren, F. Biscarini, A. Bonfiglio, C. A. Bortolotti, C. D. Frisbie, E. Macchia, G. G. Malliaras, I. McCulloch, M. Moser, T.-Q. Nguyen, R. M. Owens, A. Salleo, A. Spanu, L. Torsi, *Nat. Rev. Methods Primers* **2021**, *1*, 66.
[15] Y. Wang, Q. Gong, Q. Miao, *Mater. Chem. Front.* **2020**, *4*, 3505.
[16] a) J. Cai, J. L. Sessler, *Chem. Soc. Rev.* **2014**, *43*, 6198; b) L. M. Eytel, H. A. Fargher, M. M. Haley, D. W. Johnson, *Chem. Commun.* **2019**, *55*, 5195; c) W. Zhao, B. Qiao, C.-H. Chen, A. H. Flood, *Angew. Chem., Int. Ed.* **2017**, *56*, 13083; d) S. Pal, T. K. Ghosh, R. Ghosh, S. Mondal, P. Ghosh, *Coord. Chem. Rev.* **2020**, *405*, 213128.
[17] S. Lee, C.-H. Chen, A. H. Flood, *Nat. Chem.* **2013**, *5*, 704.
[18] B. Qiao, J. R. Anderson, M. Pink, A. H. Flood, *Chem. Commun.* **2016**, *52*, 8683.
[19] a) E. M. Zahran, E. M. Fatila, C.-H. Chen, A. H. Flood, L. G. Bachas, *Anal. Chem.* **2018**, *90*, 1925; b) E. Zeynaloo, E. M. Zahran, E. M. Fatila, A. H. Flood, L. G. Bachas, *Anal. Chem.* **2021**, *93*, 5412.
[20] a) S. Yuvaraja, S. G. Surya, V. Chernikova, M. T. Vijjapu, O. Shekhah, P. M. Bhatt, S. Chandra, M. Eddaoudi, K. N. Salama, *ACS Appl. Mater. Interfaces* **2020**, *12*, 18748; b) H. Chen, Y. Guo, G. Yu, Y. Zhao, J. Zhang, D. Gao, H. Liu, Y. Liu, *Adv. Mater.* **2012**, *24*, 4618.
[21] P. J. Leenaers, H. van Eersel, J. Li, M. M. Wienk, R. A. J. Janssen, *Macromolecules* **2020**, *53*, 7749.
[22] I. Salzmann, G. Heimel, M. Oehzelt, S. Winkler, N. Koch, *Acc. Chem. Res.* **2016**, *49*, 370.
[23] C. J. Boyle, M. Upadhyaya, P. Wang, L. A. Renna, M. Lu-Diaz, S. Pyo Jeong, N. Hight-Huf, L. Korugic-Karasz, M. D. Barnes, Z. Aksamija, D. Venkataraman, *Nat. Commun.* **2019**, *10*, 2827.
[24] E. M. Fatila, M. Pink, E. B. Twum, J. A. Karty, A. H. Flood, *Chem. Sci.* **2018**, *9*, 2863.
[25] a) M. Irimia-Vladu, *Chem. Soc. Rev.* **2014**, *43*, 588; b) P. Lin, F. Yan, *Adv. Mater.* **2012**, *24*, 34.
[26] B. Lussem, C. M. Keum, D. Kasemann, B. Naab, Z. Bao, K. Leo, *Chem. Rev.* **2016**, *116*, 13714.
[27] M. Jang, H. Kim, S. Lee, H. W. Kim, J. K. Khedkar, Y. M. Rhee, I. Hwang, K. Kim, J. H. Oh, *Adv. Funct. Mater.* **2015**, *25*, 4882.
[28] L. Huang, N. Eedugurala, A. Benasco, S. Zhang, K. S. Mayer, D. J. Adams, B. Fowler, M. M. Lockart, M. Saghayezhian, H. Tahir, E. R. King, S. Morgan, M. K. Bowman, X. Gu, J. D. Azoulay, *Adv. Funct. Mater.* **2020**, *30*, 1909805.
[29] W. Melitz, J. Shen, A. C. Kummel, S. Lee, *Surf. Sci. Rep.* **2011**, *66*, 1.
[30] C. Liu, Y. Xu, Y.-Y. Noh, *Mater. Today* **2015**, *18*, 79.
[31] a) P. A. Bobbert, A. Sharma, S. G. J. Mathijssen, M. Kemerink, D. M. De Leeuw, *Adv. Mater.* **2012**, *24*, 1146; b) M. E. Roberts, S. C. B. Mannsfeld, N. Queraltó, C. Reese, J. Locklin, W. Knoll, Z. Bao, *Proc. Natl. Acad. Sci. U. S. A.* **2008**, *105*, 12134.
[32] a) M. A. Shannon, P. W. Bohn, M. Elimelech, J. G. Georgiadis, B. J. Marinas, A. M. Mayes, *Nature* **2008**, *452*, 301; b) N. Gruber, J. N. Galloway, *Nature* **2008**, *451*, 293; c) E. T. Urbansky, *Environ. Sci. Pollut. Res.* **2002**, *9*, 187.
[33] M. D. Angione, S. Cotrone, M. Magliulo, A. Mallardi, D. Altamura, C. Giannini, N. Cioffi, L. Sabbatini, E. Fratini, P. Baglioni, *Proc. Natl. Acad. Sci. U. S. A.* **2012**, *109*, 6429.
[34] S. Mao, H. Pu, J. Chang, X. Sui, G. Zhou, R. Ren, Y. Chen, J. Chen, *Environ. Sci. Nano* **2017**, *4*, 856.
[35] X. Chen, H. Pu, Z. Fu, X. Sui, J. Chang, J. Chen, S. Mao, *Environ. Sci. Nano* **2018**, *5*, 1990.
[36] L. Barhoumi, A. Baraket, N. M. Nooredeen, M. B. Ali, M. N. Abbas, J. Bausells, A. Errachid, *Electroanalysis* **2017**, *29*, 1586.
[37] J. M. Racicot, T. L. Mako, A. Olivelli, M. Levine, *Sensors* **2020**, *20*, 2766.
[38] M. M. Grand, G. S. Clinton-Bailey, A. D. Beaton, A. M. Schaap, T. H. Johengen, M. N. Tamburri, D. P. Connelly, M. C. Mowlem, E. P. Achterberg, *Front. Mar. Sci.* **2017**, *4*, 255.
[39] a) M. Bralić, *Int. J. Electrochem. Sci.* **2018**, *13*, 1390; b) H. J. Kim, J. W. Hummel, K. A. Sudduth, S. J. Birrell, *Trans. ASABE* **2007**, *50*, 415.
[40] a) X. Jia, D. Chen, L. Bin, H. Lu, R. Zhang, Y. Zheng, *Sci. Rep.* **2016**, *6*, 27728; b) G. Zhou, B. Jin, Y. Wang, Q. Dong, A. Maity, J. Chang, R. Ren, H. Pu, X. Sui, S. Mao, J. Chen, *Mol. Syst. Des. Eng.* **2020**, *5*, 936; c) K. S. Bhat, U. T. Nakate, J. Y. Yoo, Y. Wang, T. Mahmoudi, Y. B. Hahn, *ACS Omega* **2019**, *4*, 8373.